60% Efficient Monolithically Wavelength-Stabilized 970-nm DBR Broad-Area Lasers

Paul Crump, *Senior Member, IEEE*, Md. Jarez Miah, *Member, IEEE*, Martin Wilkens, Jörg Fricke, Hans Wenzel, and Andrea Knigge

***Abstract*—Progress in epitaxial design is shown to enable increased optical output power P_{opt} and power conversion efficiency η_{E} and decreased lateral far-field divergence angle in GaAs-based distributed Bragg reflector (DBR) broad-area (BA) diode lasers. We show that the wavelength-locked power can be significantly increased (saturation at high bias current is mitigated) by migrating from an asymmetric large optical cavity (ASLOC) based laser structure to a highly asymmetric (extreme-triple-asymmetric (ETAS)) layer design. For wavelength-stabilization, 7th order, monolithic DBRs are etched on the surface of fully grown epitaxial layer structures. The investigated ETAS reference Fabry-Pérot (FP) BA lasers without DBRs and with 200 µm stripe width and 4 mm cavity length provide $P_{\mathrm{opt}} = 29$ W (still increasing) at 30 A in continuous-wave mode at room temperature, in contrast to the maximum $P_{\mathrm{opt}} = 24$ W (limited by strong power saturation) of baseline ASLOC lasers. The reference ETAS FP lasers also deliver over 10% higher η_{E} at $P_{\mathrm{opt}} = 24$ W. On the other hand, in comparison to the wavelength-stabilized ASLOC DBR lasers, ETAS DBR lasers show a peak power increment from 14 W to 22 W, and an efficiency increment from 46% to 60% at $P_{\mathrm{opt}} = 14$ W. A narrow spectral width (< 1 nm at 95% power content) is maintained across a very wide operating range. Consistent with earlier studies, a narrower far-field divergence angle and consequently an improved beam-parameter product is also observed, compared to the ASLOC-based lasers.**

***Index Terms*—Beam parameter product, beam quality, broad-area lasers, DBR lasers, far-field, high power lasers, near-field, semiconductor lasers, wavelength-stabilized lasers.**

I. Introduction

HIGH efficiency and high power GaAs-based semiconductor lasers (SLs) are nowadays crucial components in numerous scientific and industrial applications due to their low production cost and small size. In many cases they are used directly, e.g., in many direct-diode material processing applications, or for pumping solid-state and fiber lasers [1]–[3]. In high-power, kW-class applications, single SL elements are arranged in a lateral array in 1-cm bar format and subsequently stacked together vertically. Thus, single SLs with high optical power P_{opt}, high electrical-to-optical power conversion efficiency η_{E} and narrow beam divergence angle θ are preferred to simplify the overall pumping system and to reduce the system cost in \$/W. Broad-area (BA) lasers with centroid wavelength around $\lambda = 970$ nm delivering $P_{\mathrm{opt}} > 10$ W at $\eta_{\mathrm{E}} > 65\%$ in continuous-wave (CW) operation mode at room temperature have already been realized for diode lasers with stripe width around $w = 90 \ldots 100$ µm (reviewed in [4]). More recent efforts have focused on diode lasers with wider stripes $w \approx 200$ µm, allowing higher peak $P_{\mathrm{opt}} \sim 18 \ldots .20$ W at the cost of degraded beam quality [5], [6]. However, these BA lasers with Fabry-Perot (FP) cavity operate with broad spectral width $\Delta\lambda_{95\%} \sim$ 3-6 nm (at 95% power content) and a centroid wavelength which shifts strongly with increasing operating temperature at a rate $\mathrm{d}\lambda/\mathrm{d}T = 0.3$-0.4 nm/K. Applications which require narrow spectral width cannot be directly addressed by such diode lasers, for example the pumping of narrow absorption lines around $\lambda = 970 \ldots 980$ nm in Yb-doped fibers and solid state crystals [7]–[10].

Various techniques to narrow $\Delta\lambda_{95\%}$ are reviewed in [11]–[13]. Such techniques utilize either external feedback mechanisms, for example volume Bragg grating [12], [13], or internal wavelength-stabilizing mechanisms [11], such as distributed feedback (DFB) and distributed Bragg reflector (DBR). Approaches based on external stabilization techniques are now in wide use in industry [14], [15], but require more complex and expensive optical components. They also make the overall system sensitive to mechanical disturbances and suffer from early device failure due to reflection effects [16]. Internal monolithic wavelength-stabilization approaches are highly attractive for lower-cost systems with higher reliable power, if the overall efficiency remains in an acceptable range.

DBRs etched on fully grown epitaxial layer structure have been proven as an effective technique to yield narrow and temperature-stable emission [12], [17]–[19]. Recently, 130 µm wide DBR BA lasers delivering $P_{\mathrm{opt}} = 14$ W at $\eta_{\mathrm{E}} = 47\%$ have been reported at $T_{\mathrm{HS}} = 25$ °C heat-sink temperature in CW mode [20]. Here we present recent progress in the design and technological development of DBR BA lasers for increased efficiency and power, expanding on our previous brief conference presentation [19]. We show that by introducing a highly asymmetric epitaxial layer structure, P_{opt} and η_{E} can be increased with a simultaneous reduction of lateral beam divergence angle and beam-parameter product. This results in DBR-stabilized diode lasers that provide narrow and stable emission with increased $\eta_{\mathrm{E}} = 60\%$ at $P_{\mathrm{opt}} = 14$ W and operate with increased peak (rollover) power of $P_{\mathrm{opt}} > 20$ W.

Manuscript received March 4, 2022; accepted April 6, 2022. Date of publication April 14, 2022; date of current version April 27, 2022. *(Corresponding author: Md. Jarez Miah.)*

The authors are with the Ferdinand-Braun-Institut gGmbH, Leibniz-Institut für Höchstfrequenztechnik, 12489 Berlin, Germany (e-mail: paul.crump@fbh-berlin.de; jarez.miah@fbh-berlin.de; martin.wilkens@fbh-berlin.de; wenzel@fbh-berlin.de; andrea.knigge@fbh-berlin.de).

Digital Object Identifier 10.1109/JPHOT.2022.3166591

II. Device Structure

We investigate and compare BA lasers, both with and without DBRs, that use two different epitaxial layer structures. We use an asymmetric large optical cavity (ASLOC) epitaxial layer design from [4], [21] as a baseline, that is established in previous studies as being suitable for realizing highly efficient diode with monolithically integrated gratings [22]–[23]. We next introduce gratings into an improved extreme-triple-asymmetric (ETAS) laser structure from [21], which achieves higher power and conversion efficiency. Both structures contain a single InGaAs quantum well (QW) and are designed for lasing emission at $\lambda \sim$ 970 nm at $T_{\rm HS} = 25$ °C. As reported in [4], [21], 90 µm wide BA lasers with $L = 4$ mm with the baseline ASLOC design provide high $P_{\rm opt}$ and a high maximum $\eta_{\rm E} = 65\%$. However, the peak $P_{\rm opt}$ is limited by a strong reduction in slope efficiency at high operating current $I_{\rm opt}$.

The overall design approach and performance benefit of ETAS designs for increased efficiency and power has been described in detail in previous studies [21], [24]–[25]. Three main design changes are implemented in the investigated ETAS layer structure as compared with the baseline ASLOC (see [19], [21]).

First, in the ETAS design, a higher Al-content x in the surrounding $Al_xGa_{1-x}As$ waveguide layers (WLs) is used to increase the energy barrier ΔE against electron to escape from the active region into the WLs (ΔE is defined as the energy offset between the conduction band and the lowest confined state in the QW). Specifically, $\Delta E = 8.5\ k_{\rm B}T_{\rm HS}$ for the ASLOC and $12\ k_{\rm B}T_{\rm HS}$ for the ETAS structure (where $k_{\rm B}$ is the Boltzmann constant).

Second, a thinner p-doped WL is used to reduce optical losses and also to reduce electrical series resistance $R_{\rm s}$. The thin WL limits the impact of the band bending effects shown in [26] and decreases the associated additional carrier escape into the WLs at high $I_{\rm opt}$. Specifically, the thicknesses of the p-doped WLs in the investigated ASLOC and ETAS structures are 760 nm and 210 nm, respectively ($\sim$ 70% thinner in the ETAS structure).

Finally, an additional asymmetric graded-index layer pair is used surrounding the active region to maintain a sufficiently high modal gain for low threshold current. Specifically, a confinement factor $\Gamma = 0.62\%$ in the ETAS structure is achieved, comparable to the $\Gamma = 0.67\%$ of the ASLOC structure (7 nm thick QW in both cases).

The effectiveness of the ETAS-based design for higher $P_{\rm opt}$ and $\eta_{\rm E}$ at high $I_{\rm opt}$, over ASLOC-based structures has been demonstrated in single BA lasers at $\lambda = 970$ nm [21] and in 1-cm laser bars at $\lambda = 940$ nm [27]–[29]. In this paper, we evaluate the performance of wavelength-stabilized BA lasers at $\lambda = 970$ nm realized employing the above-described baseline ASLOC and ETAS structures, following on from [19].

The peak reflectivity of the grating section was first calculated using the CAMFR tool following [18], for a 7th order grating with $L_{\rm DBR} = 1$ mm length for the grating dimensions $w_{\rm groove}$ (width of groove tip closest to active region) and $d_{\rm res}$ (residual thickness, i.e., vertical offset between groove tip and active region). Results are shown in Fig. 1(a) and (b) for the ETAS and the baseline ASLOC structures, respectively. For a typical

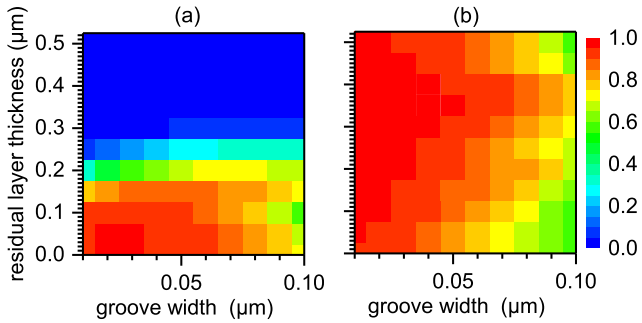

Fig. 1. Linearly-scaled false color-map of calculated peak reflectivity as a function of groove dimensions for a 1 mm long 7th order DBR grating for the investigated (a) ETAS and (b) baseline ASLOC structures.

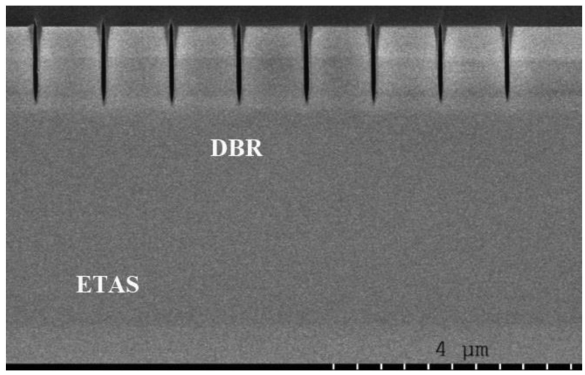

Fig. 2. Scanning electron microscope (SEM) image of a cross-section of the grating region within an ETAS DBR laser.

$w_{\rm groove} = 20\ \ldots\ 30$ nm, a DBR reflectivity of $R_{\rm DBR} > 80\%$ is achievable with $d_{\rm res} = 0\ \ldots\ 500$ nm for the ASLOC design, but with just $d_{\rm res} = 0\ \ldots\ 100$ nm for the ETAS design. The resulting $\sim$ 5-fold reduction in the process window requires much higher precision in the etching conditions for the ETAS structure.

The ASLOC and ETAS designs are realized using metal-organic vapor-phase epitaxy techniques, and processed into high power BA lasers using standard techniques. Following the calculation in Fig. 1, for wavelength-stabilization, monolithic surfaced-etched 7th order DBRs are integrated into the wafer process [18]. The realized DBR BA lasers have $w = 200$ µm wide stripe and $L = 4$ mm long cavity. The length of the unpumped, passive DBR section is $L_{\rm DBR} = 1$ mm. The DBRs are defined using electron beam lithography and etched using reactive ion etching at the rear side of the laser cavity. A scanning electron microscope (SEM) image of the DBR section within a completed ETAS DBR laser is shown in Fig. 2. The width of the grooves $w_{\rm groove}$ and the residual layer thickness $d_{\rm res}$ above the active region are chosen to ensure high reflectivity at the desired grating wavelength $\lambda \sim 970$ nm. Specifically, residual thicknesses of $d_{\rm res} = 95$ nm and 446 nm were realized for the ETAS and ASLOC material, respectively, as needed to realize $R_{\rm DBR} > 80\%$ following Fig. 1.

To clearly reveal the performance impact of the introduction of the DBR grating BA lasers, reference Fabry-Pérot (FP) BA lasers (i.e., without DBRs) with $w = 200$ µm and $L = 4$ mm

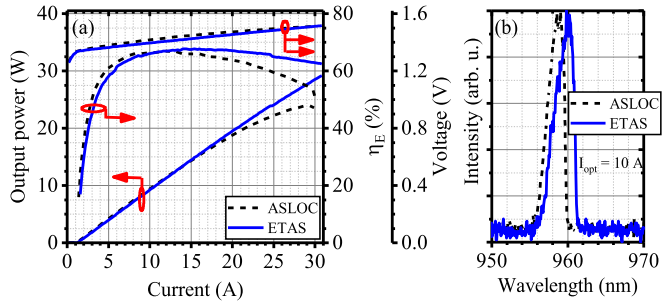

Fig. 3. (a) Output power, power conversion efficiency η_E and voltage as a function of the operating current I_{opt} of an ASLOC (dashed) and an ETAS (solid) reference FP laser in CW mode at $T_{HS} = 25$ °C. (b) Emission spectra of the lasers at $I_{opt} = 10$ A operating current.

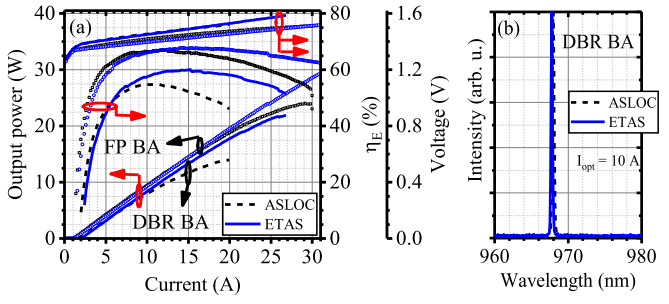

Fig. 4. (a) Output power, power conversion efficiency η_E and voltage as a function of the operating current I_{opt} of an ASLOC (dashed) and an ETAS (solid) DBR BA laser. Results of the reference BA lasers are redrawn from Fig. 3(a) (empty circle: ETAS, empty square: ASLOC). (b) Emission spectra of the DBR BA lasers at $I_{opt} = 10$ A.

are also fabricated. After complete processing, the facets of all the reference and DBR BA lasers are passivated. The front and rear facet reflectivity $R_f = 2\%$ and $R_r = 98\%$ for the reference BA lasers and $R_f = 2\%$ and $R_r < 0.1\%$ for the DBR BA lasers. To efficiently remove heat during CW operation, the lasers are soldered epi-side down onto an expansion match CuW carrier whose temperature is regulated using a TEC, itself clamped to a water cooled copper block for heat removal. All the measurements presented in this paper are performed at $T_{HS} = 25$ °C in CW mode, with the rear edge of the CuW carrier held at temperature for a thermal resistance of $R_{th} \sim 2.3$ K/W for FP BA lasers.

III. Experimental Results

First, we evaluate the improvement in the P_{opt} and η_E of the ETAS structure in comparison to the baseline ASLOC design. Fig. 3(a) shows output power-current-voltage (PIU) characteristics and η_E of the reference FP BA lasers from the baseline ASLOC and ETAS structures. The ETAS laser shows a slightly higher threshold current I_{thr} due to the lower modal gain ($\Gamma = 0.62\%$ vs. 0.67%). Although both lasers provide a similar maximum $\eta_E \sim 67\%$ and show a comparable slope efficiency η_{slope} up to $I_{opt} = 15$ A, both η_{slope} and η_E deviate strongly at higher bias I_{opt}. The ASLOC lasers produce a maximum $P_{opt} = 24$ W and $\eta_E = 54\%$ at $I_{opt} = 30$ A. In contrast, the ETAS lasers yield $P_{opt} = 29$ W (still increasing) at $I_{opt} = 30$ A, with $\eta_E = 65\%$ at $P_{opt} = 24$ W, comparable to the efficiency reported in [5] (65% at 25 W). A high $\eta_E = 63\%$ is also maintained at 30 A. In addition, as shown in Fig. 3(b), both the reference BA lasers produce broad emission spectra with $\Delta\lambda_{95\%} > 3.5$ nm around $\lambda \sim 958$ nm at $I_{opt} = 10$ A. $\Delta\lambda_{95\%}$ also changes strongly with varying I_{opt} (cf. Fig. 5(b)).

Fig. 4(a) shows the PIU characteristics and η_E of the baseline ASLOC and ETAS DBR lasers. The results of the reference BA lasers are redrawn from Fig. 3(a) for convenience. Although broadly similar trends are seen to the FP lasers, voltage and threshold current are increased, and efficiency and peak power are reduced by the introduction of the DBR region. The peak P_{opt} of the ASLOC DBR laser is 14 W at $I_{opt} = 20$ A, limited by power saturation, and $\eta_E = 46\%$ at 14 W. In contrast, the ETAS DBR laser yields a high peak (rollover) $P_{opt} = 22$ W at

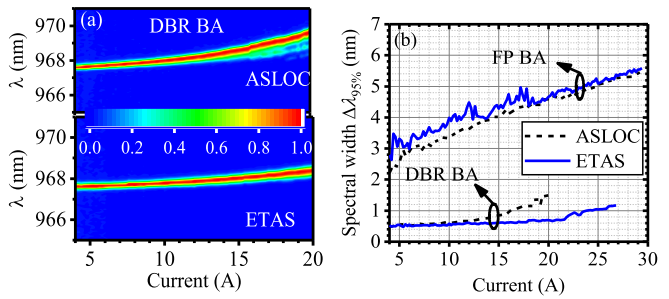

Fig. 5. (a) False-color (linearly scaled) plot of the emission spectra of the ASLOC (top) and ETAS (bottom) DBR lasers presented in Fig. 4 as a function of current. (b) Spectral width at 95% power content of the reference and DBR BA lasers as a function of the operating current I_{opt}. Solid and dashed lines represent the ETAS and ASLOC lasers, respectively.

$I_{opt} = 27$ A, where $\eta_E = 52\%$ and $\eta_E > 60\%$ is maintained up to $P_{opt} = 14$ W, significantly higher values than reported previously [18], [20].

We attribute the lower power and efficiency to two main effects. First, for the same overall chip dimension, the DBR lasers have a shorter pump length (here $L_{pump} = L - L_{DBR} = 3$ mm) compared to the reference lasers ($L_{pump} = 4$ mm), leading to (4/3)× higher R_s (also thermal resistance R_{th}) for higher voltage and ∼ 1.4× higher mirror loss $\alpha_m = (0.5/L_{pump})\ln(R_r \times R_f)$ for higher threshold current. The introduction of the monolithic grating stabilization also leads to higher threshold current and more rapid thermal rollover due to detuning effects [22]: the gain wavelength varies with temperature at 0.34 nm/K and the grating (DBR) wavelength at 0.077 nm/K, meaning that gain and grating can only overlap at one operating point. Here, gain and grating coincide at around $P_{opt} = 15$ W, threshold current is increased and thermal rollover is exaggerated due to reduced gain away from this point.

Fig. 4(b) and 5(a) present the emission spectra of the DBR BA lasers at $I_{opt} = 10$ A and false color-map of the emission spectra as a function of I_{opt}, respectively. The DBR lasers produce a slowly changing emission wavelength around the grating wavelength $\lambda \sim 968$ nm with 4-5× narrower $\Delta\lambda_{95\%}$ than the reference BA lasers (cf. Figs. 3(b), 4(b) and 5(b)). As presented in Fig. 5(b), the ETAS DBR laser shows $\Delta\lambda_{95\%} \leq$ 1 nm up to 25 A operating current.

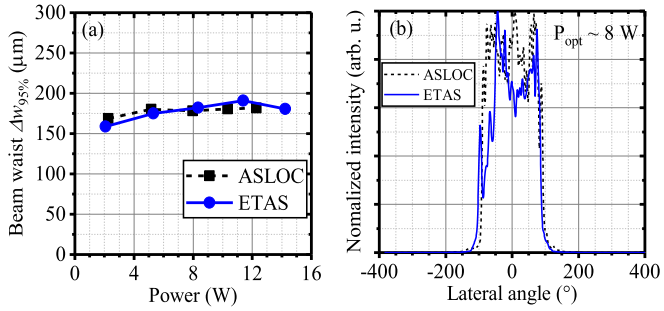

Fig. 6. (a) Lateral beam waist at 95% power content of the baseline ASLOC (square, dashed) and the ETAS (circle, solid) DBR lasers as a function of operating power $P_{\rm opt}$. (b) Near-field profiles of the lasers at $P_{\rm opt} \sim 8$ W.

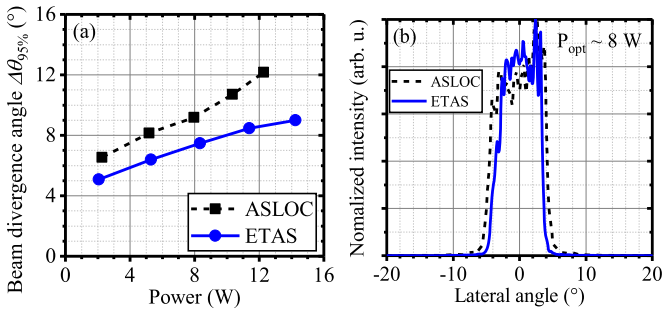

Fig. 7. (a) Lateral far-field angle at 95% power content of the baseline ASLOC (square, dashed) and the ETAS (circle, solid) DBR lasers as a function of operating power $P_{\rm opt}$. (b) Lateral far-field profiles of the lasers at $P_{\rm opt} \sim 8$ W.

DBR BA lasers must demonstrate not just high $P_{\rm opt}$ and $\eta_{\rm E}$ but also narrow in-plane far field angle to find effective application. Figs. 6 and 7 therefore compare the measured near-field and far-field properties of the DBR lasers presented in Figs. 4 and 5. Figs. 6(a) and 7(a) present the beam waist $\Delta w_{95\%}$ and far-field divergence angle $\Delta\theta_{95\%}$ at 95% power content at different $P_{\rm opt}$ up to 12-14 W of the ASLOC and ETAS DBR lasers. Figs. 6(b) and 7(b) present their near-field and far-field distributions at $P_{\rm opt} \sim 8$ W. Both the ASLOC and ETAS DBR lasers produce near-field distributions with similar beam waist close to the stripe width of 200 μm, with $\Delta w_{95\%}$ varying within 160 μm - 190 μm range. However, the ETAS DBR laser shows narrower far-field profiles with 1.7-4° reduced beam divergence angle, for example, $\Delta\theta_{95\%} = 7.5°$ for the ETAS DBR laser and $\Delta\theta_{95\%} = 9.2°$ for the ASLOC laser at $P_{\rm opt} \sim 8$ W.

Next, the lateral beam-parameter product $BPP_{\rm lat} = 0.25 \times \Delta w_{95\%} \times \Delta\theta_{95\%}$ is obtained from the data in Figs. 6 and 7 and is presented in Fig. 8. The measured data points are fitted with a linear empirical fit $BPP_{\rm lat} = BPP_0 + S_{\rm th}\Delta T$, following [30], where ΔT is the increase of the average temperature in the active region over $T_{\rm HS}$ (calculated by multiplying the dissipated power within the device by the thermal resistance). BPP_0 represents the non-thermal background of the $BPP_{\rm lat}$ which include contributions from all the effects nearly unaffected with temperature change, e.g., process or packaging related waveguiding [31]. The second term in the fit equation describes the change of the $BPP_{\rm lat}$ due to internal heating, with $S_{\rm th}$ representing the rate.

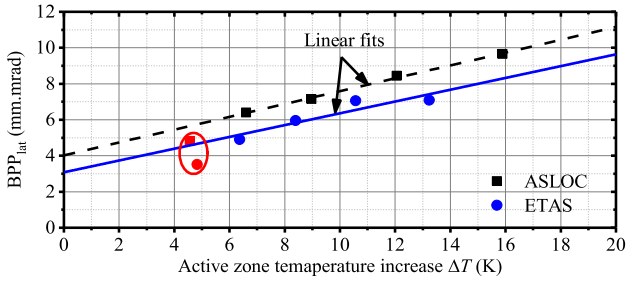

Fig. 8. Lateral beam parameter product $BPP_{\rm lat}$ for the ASLOC (square) and the ETAS (circle) DBR lasers, calculated from Figs. 6(a) and 7(a), as function of the active zone temperature increase ΔT. Solid lines are the linear fits to the data (fit equation: $BPP_{\rm lat} = BPP_0 + S_{\rm th}\Delta T$). Data points marked with red circles are excluded from the fits.

The ETAS DBR lasers show overall lower $BPP_{\rm lat}$ values, as illustrated in Fig. 8, due to the reduced far-field angle. A lower $BPP_0 = 3.08$ mm.mrad is obtained in contrast to the $BPP_0 = 4.03$ mm.mrad for the ASLOC laser. The change of the $BPP_{\rm lat}$ with increasing ΔT is nearly identical, being slightly faster for the case of the ASLOC laser ($S_{\rm th} = 0.36$ vs. 0.33 mm.mrad/K). The reason for the lower BPP_0 for the ETAS laser requires further study: see [31]–[33]. Overall, the improvement in the $BPP_{\rm lat}$ of the ETAS DBR lasers confirms the pattern observed in the FP BA lasers without DBRs in [21].

IV. Conclusion

Highly efficient and high-power wavelength-stabilized lasers based on an improved ETAS design emitting at $\lambda \sim 970$ nm wavelength are presented. As seen in earlier studies, improved peak $P_{\rm opt}$ and $\eta_{\rm E}$ at high $I_{\rm opt}$ is achieved by mitigating the power saturation effects seen at high $I_{\rm opt}$ in the baseline ASLOC design. Stable and narrow emission spectra are obtained by the successful introduction of monolithic surface-etched DBRs into the epitaxial laser structure. The resulting ETAS DBR lasers provide more than 20 W at $\eta_{\rm E} = 52\%$, while maintaining a high $\eta_{\rm E} > 60\%$ up to $P_{\rm opt} = 14$ W. Power and efficiency in these ETAS devices exceed the previously best reported numbers ($\eta_{\rm E} = 47\%$ from 130 μm wide DBR laser at $P_{\rm opt} = 14$ W) and the (here presented) baseline ASLOC DBR laser ($\eta_{\rm E} = 46\%$). The ETAS DBR lasers also show reduced lateral far-field angle and thus improved $BPP_{\rm lat}$, confirming a similar trend previously observed for conventional BA lasers without DBRs [21]. Further improvement in the $P_{\rm opt}$ and $\eta_{\rm E}$ are feasible by implementing DBR regions with higher reflectivity, and by further optimizing the ETAS structure for high modal gain [34] to reduce the losses incurred by longitudinal spatial hole burning [35].

References

[1] Y. Zou *et al.*, "Reliability and performance of InGaAs broad area lasers emitting between 910-980 nm," *Proc. SPIE*, vol. 4285, pp. 159–164, 2001.
[2] S. G. Strohmaier *et al.*, "Forward development of kW-class power diode laser bars," *Proc. SPIE*, vol. 10514, 2018, Art. no. 1051409.
[3] S. D. McDougall *et al.*, "Advances in diode laser bar power and reliability for multi-kW disk laser pump sources," *Proc. SPIE*, vol. 11262, 2020, Art. no. 1126206.
[4] P. Crump *et al.*, "Efficient high-power laser diodes," *IEEE J. Sel. Topics Quantum Electron.*, vol. 19, no. 4, Jul./Aug. 2013, Art. no. 1501211.

[5] Y. Yamagata, Y. Kaifuchi, R. Nogawa, K. Yoshida, R. Morohashi, and M. Yamaguchi, "Highly efficient 9xx-nm band single emitter laser diodes optimized for high output power operation," *Proc. SPIE*, vol. 11262, 2020, Art. no. 1126203.

[6] Y. Xiong *et al.*, "Advances in 976nm single emitter broad area semiconductor diode lasers for 300W+ fiber laser pump module applications," *Proc. SPIE*, vol. 11983, 2022, Art. no. 11983-4.

[7] V. Gapontsev *et al.*, "Highly-efficient high-power pumps for fiber lasers," *Proc. SPIE*, vol. 10086, 2017, Art. no. 1008604.

[8] H. M. Pask *et al.*, "Ytterbium-doped silica fiber lasers: Versatile sources for the 1-2 μm region," *IEEE J. Sel. Topics Quantum Electron.*, vol. 1, no. 1, pp. 2–13, Apr. 1995.

[9] M. Siebold *et al.*, "Yb:CaF_2—A new old laser crystal," *Appl. Phys. B*, vol. 97, no. 2, pp. 327–338, 2009.

[10] M. Kahle, J. Körner, J. Hein, and M. C. Kaluza, "Performance of a quantum defect minimized disk laser based on cryogenically cooled Yb:CaF_2," *Opt. Laser Technol.*, vol. 92, pp. 19–23, 2017.

[11] P. Crump *et al.*, "High power and high efficiency monolithic edge-emitting Gaas-based lasers with narrow spectral widths," in *Advances in Semicondcutpr Lasers*, J. J. Coleman, A. C. Bryce, and C. Jagadish, Eds., vol. 86, 2012, pp. 85–91.

[12] P. Crump *et al.*, "High-power laser diodes for direct applications and laser pumping," in *Advances in High-Power Fiber and Diode Laser Engineering*, I. Divliansky, Ed., 2019, pp. 89–125.

[13] S. Hengesbach, "Spektrale stabilisierung und inkohärente überlagerung von diodenlaserstrahlung mit volumenbeugungsgittern," Ph.D. dissertation, RWTH Aachen Univ., Germany, Shaker Verlag, 2014.

[14] N. Moshegov *et al.*, "Highly-efficient high-power pumps for QCW fiber lasers," *Proc. SPIE*, vol. 10900, 2019, Art. no. 109000G.

[15] T. Könning *et al.*, "Wavelength stabilized fiber coupled modules at 79x nm, 88x nm, and 97x nm with up to 600W output power based on single emitters," *Proc. SPIE*, vol. 11668, 2021, Art. no. 116680F.

[16] H. Kissel, B. Leonhaeuser, J. W. Tomm, M. Hempel, and J. Biesenbach, "Accelerated degradation of high power diode lasers caused by external optical feedback operation," in *Proc. IEEE Int. Semicond. Laser Conf.*, 2018, pp. 1–2.

[17] J. Fricke, H. Wenzel, M. Matalla, A. Klehr, and G. Erbert, "980-nm DBR lasers using higher order gratings defined by i-line lithography," *Semicond. Sci. Technol.*, vol. 20. no. 11, pp. 1149–1152, 2005.

[18] J. Fricke *et al.*, "Surface Bragg gratings for high brightness lasers," *Proc. SPIE*, vol. 11301, 2020, Art. no. 113011H.

[19] P. Crump *et al.*, "970 nm DBR broad-area semiconductor lasers with 60% conversion efficiency," in *Proc. 27th Int. Semicond. Laser Conf.*, Potsdam, Germany, 2021, Art. no. WP3.6.

[20] R. Paoletti *et al.*, "High power wavelength stabilized multiemitter semiconductor laser module using highly manufacturable DBR diode lasers," *Proc. SPIE*, vol. 11262, 2020, Art. no. 112620K.

[21] A. Boni, S. Arslan, G. Erbert, P. Della Casa, D. Martin, and P. Crump, "Epitaxial design progress for high power, efficiency, and brightness in 970 nm broad area lasers," *Proc. SPIE*, vol. 11668, 2021, Art. no. 1166807.

[22] P. Crump, C. M. Schultz, H. Wenzel, G. Erbert, and G. Tränkle, "Efficiency-optimized monolithic frequency stabilization of high-power diode lasers," *J. Phys. D: Appl. Phys.*, vol. 46, no. 1, 2013, Art. no. 013001.

[23] J. Decker, J. Fricke, A. Maaßdorf, G. Erbert, and P. Crump, "High power surface-grating stabilized narrow-stripe broad area lasers with beam parameter product < 2 mm$\times$mrad," in *Proc. Conf. Lasers Electro-Opt.: Sci. Innovations*, San Jose, USA, 2016, Art. no. SW4M.6.

[24] K. H. Hasler *et al.*, "Comparative theoretical and experimental studies of two designs of the high-power diode lasers," *Semicond. Sci. Technol.*, vol. 29, no. 4, 2014, Art. no. 045010.

[25] T. Kaul, G. Erbert, A. Maaßdorf, S. Knigge, and P. Crump, "Suppressed power saturation due to optimized optical confinement in 9xx nm high-power diode lasers that use extreme double asymmetric vertical designs," *Semicond. Sci. Technol.*, vol. 33, no. 34, 2018, Art. no. 035005.

[26] H. Wenzel, P. Crump, A. Pietrzak, X. Wang, G. Erbert, and G. Tränkle, "Theoretical and experimental investigations of the limits to the maximum output power of diode lasers," *New J. Phys.*, vol. 12, no. 8, 2010, Art. no. 085007.

[27] M. J. Miah, A. Boni, D. Martin, P. Della Casa, and P. Crump, "Highly asymmetric epitaxial designs for increased power and efficiency in kW-class gaas-based diode laser bars," in *Proc. 27th Int. Semicond. Laser Conf.*, Potsdam, Germany, 2021, Art. no. TuP2.1.

[28] M. J. Miah, A. Boni, D. Martin, A. Knigge, P. Della Casa, and P. Crump, "Killowatt-class, 1-cm diode laser bars at 910-940 nm with improved power, conversion efficiency and beam quality," *Proc. SPIE*, vol. 11983, 2022, Art. no. 11983-3.

[29] M. J. Miah, A. Boni, S. Arslan, D. Martin, P. Della Casa, and P. Crump, "Optimizing vertical and lateral waveguides of kW-class laser bars for higher peak power, efficiency and lateral beam quality," *IEEE Photon. J.*, vol. 14, no. 3, 2022, doi: 10.1109/JPHOT.2022.3165399.

[30] M. Winterfeldt, P. Crump, S. Knigge, A. Maaßdorf, U. Zeimer, and G. Erbert, "High beam quality in broad area lasers via suppression of lateral carrier accumulation," *IEEE Photon. Technol. Lett.*, vol. 27, no. 17, pp. 1809–1812, Sep. 2015.

[31] P. Crump *et al.*, "Experimental studies into the beam parameter product of Gaas high-power diode lasers," *IEEE J. Sel. Topics Quantum Electron.*, vol. 28, no. 1, Jan./Feb. 2022, Art. no. 1501111.

[32] M. Winterfeldt *et al.*, "Assessing the influence of the vertical epitaxial layer design on the lateral beam quality of high-power broad area diode lasers," *Proc SPIE*, vol. 9733, 2016, Art. no. 970330O.

[33] P. Crump *et al.*, "Novel approaches to increasing the brightness of broad area lasers," *Proc. SPIE*, vol. 9767, 2016, Art. no. 97671L.

[34] A. Boni, P. Della Casa, D. Martin, and P. Crump, "Efficiency optimization of high-power Gaas lasers by balancing confinement and threshold," in *Proc. 27th Int. Semicond. Laser Conf.*, Potsdam, Germany, 2021, Art. no. TuP2.3.

[35] S. Arslan *et al.*, "The impact of longitudinal spatial hole burning on the carrier density profile in high-power lasers," in *Proc. 27th Int. Semicond. Laser Conf.*, Potsdam, Germany, 2021, Art. no. TuP2.5.